



Effects of Rapid Heat Treatments on the Properties of Cu₂O Thin Films Deposited at Room Temperature Using an Ammonia-Free SILAR Technique

R. E. Trinidad-Urbina¹ · R. Castanedo-Pérez¹ · G. Torres-Delgado¹ · A. Sánchez-Martínez² · R. Ramírez-Bon¹ 

Received: 9 February 2024 / Accepted: 24 June 2024 / Published online: 12 July 2024
© The Author(s) 2024

Abstract

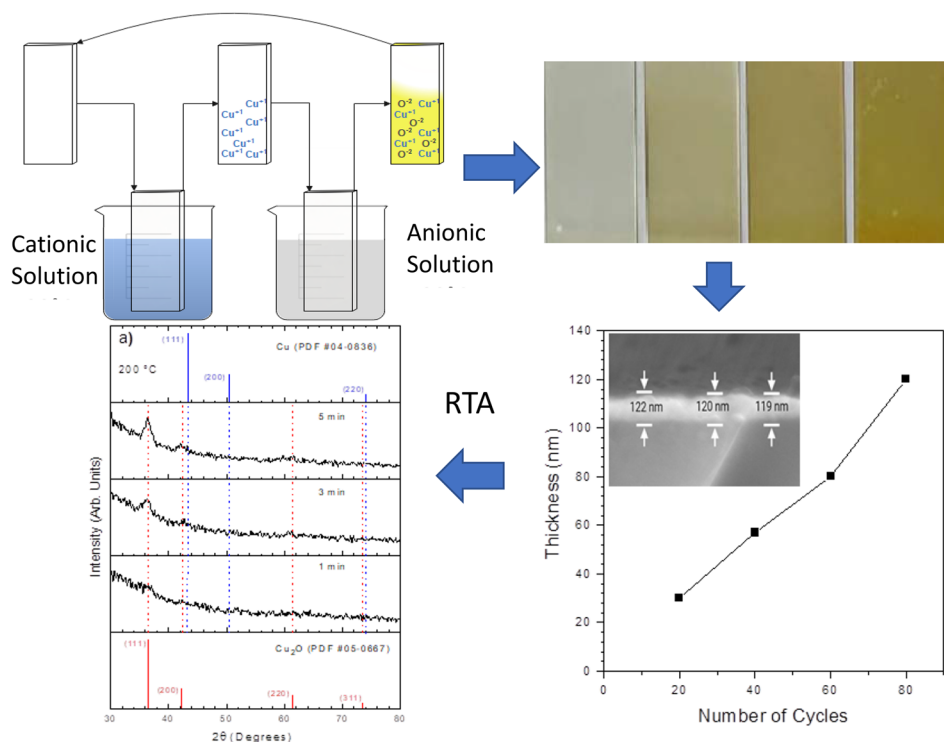
We report herein the analysis of the properties of copper(I) oxide thin films deposited by an optimized ammonium-free successive ion layer adsorption and reaction (SILAR) technique. The Cu₂O thin film deposition process was carried out at room temperature using copper acetate monohydrate, sodium citrate as complexing agent, and hydrogen peroxide as precursors of copper and oxygen ions, respectively. The harmless and easy-to-handle sodium citrate replaces the volatile NH₄OH commonly employed as complexing agent in the SILAR technique for the deposition of metal oxide thin films. The optical, structural, morphological, and electrical properties of the as-deposited Cu₂O thin films were studied as a function of the number of cycles during deposition, as well as their modifications produced by the effect of rapid thermal annealing (RTA) in vacuum in a temperature range of 200–250°C for 1 min, 3 min, and 5 min. The as-deposited thin films had cubic crystalline structure corresponding to the Cu₂O phase as determined by x-ray diffraction (XRD), with a direct energy bandgap of 2.43–2.51 eV depending on the number of cycles, and electrical resistivity of the order of 10³ Ω cm. The XRD and x-ray photoelectron spectroscopy (XPS) analysis of the Cu₂O thin films treated by RTA demonstrated an increase of the crystal size with time and temperature of the RTA and reduction effects from Cu²⁺ to Cu¹⁺ oxidation states. On the other hand, the RTA treatments also decreased their energy bandgap to 2.38 eV and electrical resistivity to 10² Ω cm. The high energy bandgap values of the Cu₂O thin films were attributed to quantum confinement effects produced by their small crystal size in the range of 3.6–8.6 nm.

✉ R. Ramírez-Bon
rrbon@cinvestav.mx

¹ Centro de Investigación y de Estudios Avanzados del IPN, Unidad Querétaro, Apdo, Postal 1-798, 76001 Querétaro, Qro., México

² Departamento de Ingeniería de Proyectos, Centro Universitario de Ciencias Exactas e Ingenierías (CUCEI), Universidad de Guadalajara, Av. José Guadalupe Zuno # 48, Industrial Los Belenes, 45157 Zapopan, Jal., México

Graphical Abstract



Keywords Chemical deposition · Cu₂O · rapid thermal annealing · ammonia-free

Introduction

Semiconductor metal oxides have a wide variety of electronic applications because of their electronic charge transport properties ascribed to the interaction between the *ns* metal and *2p* oxygen orbitals. These orbital interactions produce a significant difference in the charge transport characteristics as compared to common covalent semiconductors.¹ The electrical conductivity of semiconductor metal oxides can be either *n*- or *p*-type, with the *n*-type being the most widely studied. This is because the *p*-type semiconductor metal oxides with good electrical properties represent a challenge due to their high hole effective mass, which can be a serious drawback.^{2–5} Nevertheless, *p*-type metal oxides^{4–7} like NiO, CuO, Cu₂O, and SnO with good electrical properties have been developed for different optoelectronic applications such as photodetectors, sensors, and *p*-channel thin film transistors. One of the *p*-type metal oxide materials that recently has attracted great interest is copper oxide, which can occur in two stable crystalline forms, namely, cuprite (Cu₂O) and tenorite (CuO). Particularly, the Cu₂O phase is a semiconductor metal oxide with *p*-type electrical conductivity, energy bandgap values ranging between 2 eV and 2.6 eV, and a high absorption coefficient of electromagnetic

radiation in the visible region. Furthermore, it is abundant in nature with zero toxicity and low cost.^{8,9} Due to these characteristics, Cu₂O is a material widely used in several technological applications such as thin film transistors, solar cells, photocatalysis, light-emitting diodes, and photodiodes.^{10–13} Some properties of the Cu₂O phase favor its use over CuO for specific applications. For example, it has a direct bandgap of around 2.0 eV, which is ideal for absorbing sunlight in solar cell applications, while CuO has an indirect bandgap of about 1.2 eV, making it less efficient at absorbing sunlight. Because of the stability and high surface area of Cu₂O, it has been exploited as a catalytic material for a variety of chemical reactions, including photocatalytic water splitting, CO oxidation, and reduction of NO. On the other hand, the characteristics of the CuO phase are more suitable for use as a catalyst material in gas-sensing applications. However, in general, it is more challenging to achieve the Cu₂O phase in the form of thin films than CuO because of the higher thermodynamic stability of the latter. Indeed, Cu₂O requires more specific deposition conditions, such as lower temperatures and the use of reducing agents, to either avoid or minimize the formation of the CuO phase.

Cu₂O thin films can be deposited by different techniques such as radio-frequency (RF) sputtering,^{14,15} chemical

vapor deposition,¹⁶ electrodeposition,¹⁷ spray pyrolysis,¹⁸ dip-coating,¹⁹ chemical bath deposition (CBD),^{20,21} and successive ion layer adsorption and reaction (SILAR).^{22–27} The SILAR method is a relatively new chemical deposition method derived from CBD. The basic principle of this method for the deposition of binary compounds consists of carrying out two chemical reactions in aqueous solutions sequentially, as follows: (i) immersion of the substrate in the precursor cationic solution, where the cations of the element of interest are adsorbed on the surface of the substrate; (ii) immersion of the substrate, commonly in deionized water, for rinsing to release the excess cations not adsorbed on the surface; (iii) immersion of the substrate in the precursor anionic solution, where the anions react with the cations adsorbed on the surface and form the solid binary compound of interest; and (iv) second rinse stage where the excess ions are removed from the thin film surface. After this, one SILAR cycle is completed, producing a very thin layer of the binary compound, whose thickness can be increased in a controlled way just by repeating the cycles. The SILAR method is quite appropriate for the deposition of metal oxide semiconductors, which include ZnO, SnO₂, TiO₂, Fe₂O₃, among others.²⁸ The properties of the metal oxide thin films deposited by SILAR such as crystalline structure, grain size, thickness, and roughness depend on the concentrations of the precursor solutions, number of deposition cycles, rinsing and immersion times, etc. The advantages of the SILAR method for the deposition of metal oxide thin films include the possibility to deposit on a large area of several types of substrates at normal pressure and low temperature, the use of a simple setup with inexpensive instruments, and avoiding vacuum conditions, resulting in a low-cost process. Furthermore, the SILAR method also features great control over stoichiometry, morphology, thickness, and grain size of the deposited materials with an excellent growth rate.

There is a vast body of scientific literature, including review papers,^{22–27,29} on the deposition and characterization of copper oxide thin films using the SILAR technique. These studies focused on the understanding of the relation between the deposition parameters and the structural, morphological, optical, and electrical properties of the films, to enhance their performance in specific applications. Some of the reports also included an analysis of the influence of substrate type, annealing conditions, and post-treatment processes on the properties of the deposited copper oxide thin films. With regard to Cu₂O thin films deposited by the SILAR technique and their applications, the following is a brief review of the recent literature. Vasuhi et al.³⁰ synthesized Cu₂O thin films using copper sulphate pentahydrate, sodium thiosulfate, and sodium hydroxide at 80°C as precursors. The Cu₂O thin films were doped with tin (Sn) to improve their structural and optical properties. In addition, there is a similar work by this author where the Cu₂O material was evaluated as an

ammonium gas sensor under different doping concentrations of silver (Ag).³¹ On the other hand, Sassi et al.³² studied the performance of the heterostructure formed by Cu₂O nanoparticles deposited by SILAR and TiO₂ nanotubes in the degradation of amido black dye. The precursors for copper oxide were copper sulphate pentahydrate, sodium thiosulfate, and sodium hydroxide at 70°C, plus an extra rinsing step. Chatterjee et al.²² used CuCl₂ and NH₄OH in the cationic solution and H₂O₂ for the anionic solution with methanol for the rinsing steps to obtain thin films of the Cu₂O phase by SILAR, which was transformed to the CuO phase by thermal annealing in air at 450°C. Baig et al.²⁵ reported CuSO₄ and Na₂S₂O₃ in a cationic solution and NaOH, at several temperatures in the range of 40–80°C for the anionic solution with water for the rinsing steps. Altindemir and Gumus²⁶ studied the properties of Cu₂O thin films obtained from different copper salts in the cationic precursor solution mixed with Na₂S₂O₃ and NaOH at 60°C in an anionic solution.

Thermal treatments are often applied to thin films deposited by different techniques to achieve specific crystalline phases of copper oxide.^{33–36} In addition, these treatments can improve the general properties of the material. Among these treatments, rapid thermal annealing (RTA) has garnered increasing attention recently due to its great advantages, including sudden heating up to 1000°C for a short period, as compared to conventional treatments. This heating can be achieved by heat radiation sources such as tungsten halogen lamps, graphite heaters, and arc lamps, ranging from ultraviolet (UV) to infrared (IR).³⁷ The main advantages of RTA compared to conventional thermal processes, in which heating sources display electrical resistance, are that they are short-term treatments for a few (single) samples, ensuring better uniformity in the diffusion and activation of dopants, densification of thin films, etc., as compared with conventional steady-state thermal treatments. Furthermore, the energy consumption with RTA is lower. Also, the RTA process can be carried out under vacuum conditions or controlled inert or reactive atmospheres such as Ar, N₂, or forming gas. In a recent paper,³⁸ CuO thin films deposited by dip coating on Cd₂SnO₄ films were transformed to Cu₂O films by RTA in vacuum at temperatures in the range of 300–450°C for 10 min.

As in the CBD technique, the cationic precursor solution in SILAR also includes a complexing agent of metallic cations for better control of the thin film growth process. This is the role of NH₄OH and Na₂S₂O₃ in many papers reporting the SILAR deposition of Cu₂O thin films.^{22–27} In this regard, efforts have been made to replace toxic chemical complexing agents such as volatile NH₄OH with other compounds, which are easier to handle, cheaper, and have lower toxicity. In this work, Cu₂O thin films were deposited at room temperature by an optimized ammonium-free SILAR method using

sodium citrate as complexing agent, which, unlike NH₄OH, is a nontoxic, nonvolatile, and easy-to-handle reactant. Sodium citrate is a versatile compound with numerous applications due to its unique properties as reducing and stabilization agent, pH controller, anticoagulant, etc. Sodium citrate is very effective as a complexing (chelating) agent capturing metal ions and forming relatively stable metal complexes in aqueous solutions. The gradual release of the metal ions from these complexes plays a crucial role during thin film growth in solution. Therefore, the substitution of NH₄OH by sodium citrate in the SILAR process has great relevance due to its potential to improve the environmental impact, safety, process efficiency, and waste reduction in the thin film deposition process. The aim of this paper is to assess the properties of the Cu₂O thin films to demonstrate the viability and convenience of the ammonia-free, citrate-based SILAR method. In addition, this SILAR method is very simple because it involves only two steps: the alternating immersion of the substrate in cationic and anionic solutions. Furthermore, to improve the properties of the Cu₂O thin films obtained by SILAR at room temperature, we analyzed the effects of RTA on their structural, optical, morphological, and electrical properties.

Experimental Section

The SILAR process for the deposition of Cu₂O thin films on glass substrates consisted of two immersion steps, in cationic and anionic precursor solutions. For both steps, the solutions were at room temperature, and the immersion time was 45 s, without rinsing between steps. The cationic solution was prepared by mixing in a 100-ml beaker 30 ml of monohydrated cupric acetate (Cu(CH₃COO)₂·H₂O, > 99% purity, Golden Bell) at 0.1 M, 30 ml of sodium citrate (Na₃C₃H₅O(COO)₃, > 99% purity, Baker) at 0.1 M, and approximately 3 ml of potassium hydroxide (KOH, > 85% purity, Sigma-Aldrich) at 2 M to achieve a solution pH of 12. The anionic solution consisted of 100 ml of 1% diluted hydrogen peroxide (H₂O₂, Golden-Bell). Before the thin film deposition, the glass substrates were cleaned by washing with a sponge and liquid detergent and rinsing with deionized water. Afterward, they were placed in a glass container for slides filled with deionized water and subjected to an ultrasonic bath for 10 min. The same procedure was repeated substituting deionized water with a mixture of acetone/ethanol solvents in a 1:1 ratio. The two-step SILAR process was applied to deposit a set of four thin films at 20, 40, 60, and 80 cycles, respectively. The deposited thin films were homogeneous, very well adhered to the glass substrates, and with a dark yellowish color, as observed in the photographs of the complete set of thin films in Fig. 1. The

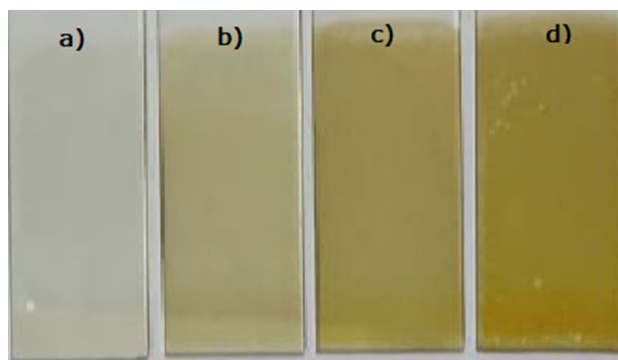


Fig. 1 Photographs of the Cu₂O thin films deposited on glass substrates (1 inch×3 inches) by SILAR at (a) 20, (b) 40, (c) 60, and (d) 80 cycles.

color of these thin films agrees with the color reported for the Cu₂O crystalline phase.³⁹

To enhance the crystalline and electrical properties of the as-deposited thin films, they were subjected to RTA in vacuum at temperatures of 200°C and 250°C for 1 min, 3 min, and 5 min. The crystalline structure of the as-deposited and annealed thin films was analyzed by x-ray diffraction (XRD) using a Rigaku D/Max 2100 diffractometer (30 kV, 16 mA) with copper CuK α radiation. The surface morphology and thickness of the samples were observed by scanning electron microscopy (SEM) using a JEOL JSM-6380LV instrument. The optical reflectance (*R*) and transmittance (*T*) spectra of the films at normal incidence were measured using a FilmTek 3000 SCI spectrophotometer in the wavelength range from 240 nm to 840 nm. The surface morphology and roughness of the thin films were determined from atomic force microscopy (AFM; Nanoscope IV Dimension 3100) images recorded in tapping mode. XPS spectra were collected using an x-ray spectrometer (Phi 5100). The high-resolution XPS spectra (HR-XPS) were collected with 15 eV pass energy and a step size of 0.05 eV. The HR-XPS spectra were aligned with the C 1s signal at 284.8 eV. Before the measurements, argon ion bombardment under ultrahigh vacuum conditions was used to clean the surface of the samples. The electrical resistivity of the Cu₂O thin films was measured by the transmission line method. For this, contact pairs of titanium with a range of distances between contacts of 40–100 μ m were deposited by the thermal evaporation technique on the thin film surface using a shadow mask. Then current versus voltage curves were measured with a Keithley 4200 semiconductor parameter analyzer in the voltage range from –5 V to 5 V.

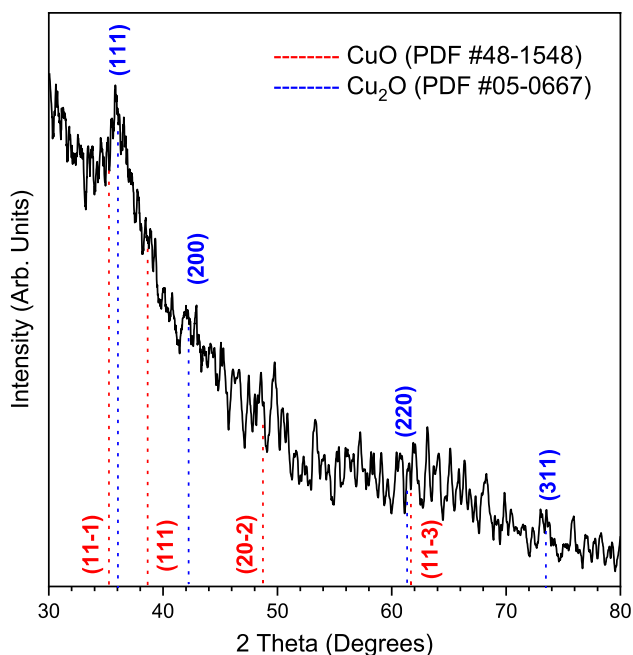


Fig. 2 XRD pattern of the Cu₂O thin film deposited at 80 cycles.

Results and Discussion

Figure 2 displays the XRD pattern of the thin film deposited at 80 SILAR cycles, where a very clear diffraction peak at 36° is observed over the noise. The red and blue dotted vertical lines indicate the 2θ angles of the diffraction peaks for the monoclinic CuO (PDF #48-1548) and cubic Cu₂O (PDF #05-0667) crystalline phases, respectively. From the comparison with these reference lines, the observed diffraction peak at 36° can be related with the (111) diffraction line of the cubic Cu₂O crystalline phase. There is no evidence in this pattern of the CuO phase, and therefore, the thin films deposited by the SILAR process can be identified as cubic Cu₂O thin films. This XRD analysis included only the thickest film deposited at 80 cycles, whose thickness is 120 nm, because the thinner films with thickness less than 100 nm, deposited at a lower number of cycles, did not show observable diffraction peaks. In Fig. 3, the thin film thickness, measured by cross-sectional SEM image analysis, as a function of the number of SILAR cycles shows a linear film growth trend with a growth rate of 1.5 nm/cycle. The cross-sectional SEM image of the 80-cycle Cu₂O thin film, in the inset of this figure, shows its uniform thickness around 120 nm. The following is a list of reactions that can explain the formation of the Cu₂O thin films in the two-step SILAR deposition process:

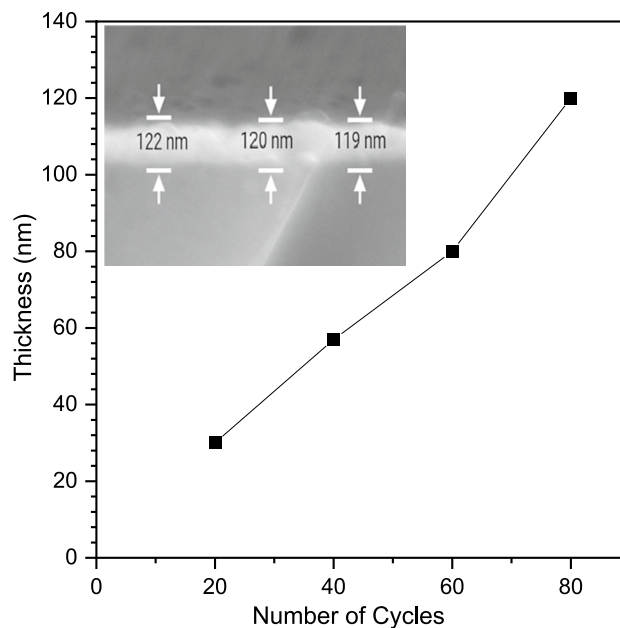
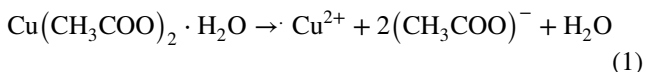
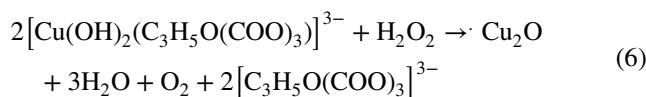
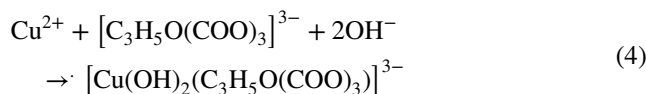
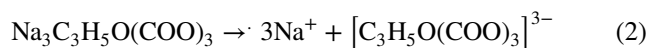


Fig. 3 Cu₂O thin film thickness versus number of cycles. The inset shows the cross-sectional SEM image of the film deposited at 80 cycles.



The reactions (1)–(4) occur in the first step, during the immersion in the cationic solution, and the reactions (5)–(6) take place in the second one during the immersion in the anionic solution, which include the formation of the Cu₂O phase after each cycle.

Figure 4a–d shows the SEM images of the Cu₂O thin films deposited at 20, 40, 60, and 80 cycles, respectively, where their surface morphology can be observed. The Cu₂O thin film surface is compact granular and homogeneous with complete coverage of the substrate. Also, the thin film surface is rather rough; only the thinnest film surface is smooth. There are no observed surface features like cracks or pin holes. The round-shaped grains tend to agglomerate in

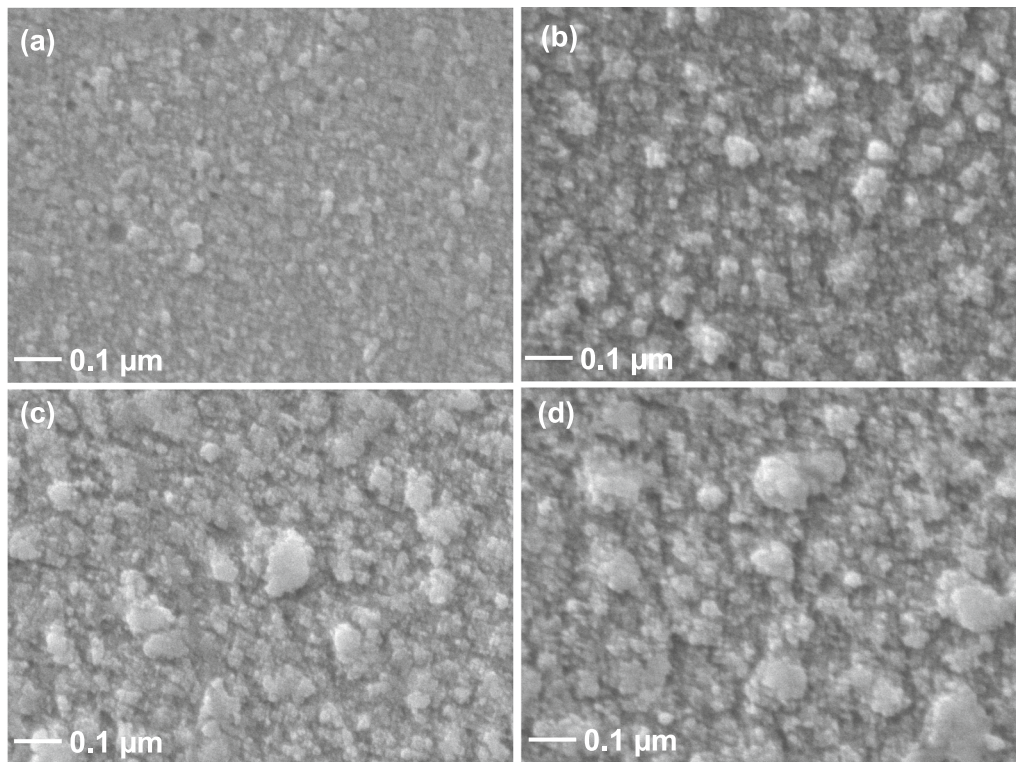


Fig. 4 SEM images of the Cu₂O thin films deposited at (a) 20, (b) 40, (c) 60, and (d) 80 cycles.

irregularly shaped particles with increasing size as the number of cycles increases, leading to rougher thin films. This is corroborated by the three-dimensional (3D) AFM images

of the set of Cu₂O thin films shown in Fig. 5a–d. The compact granular surface of the thin films displays an increasing surface roughness with the increase in the number of cycles.

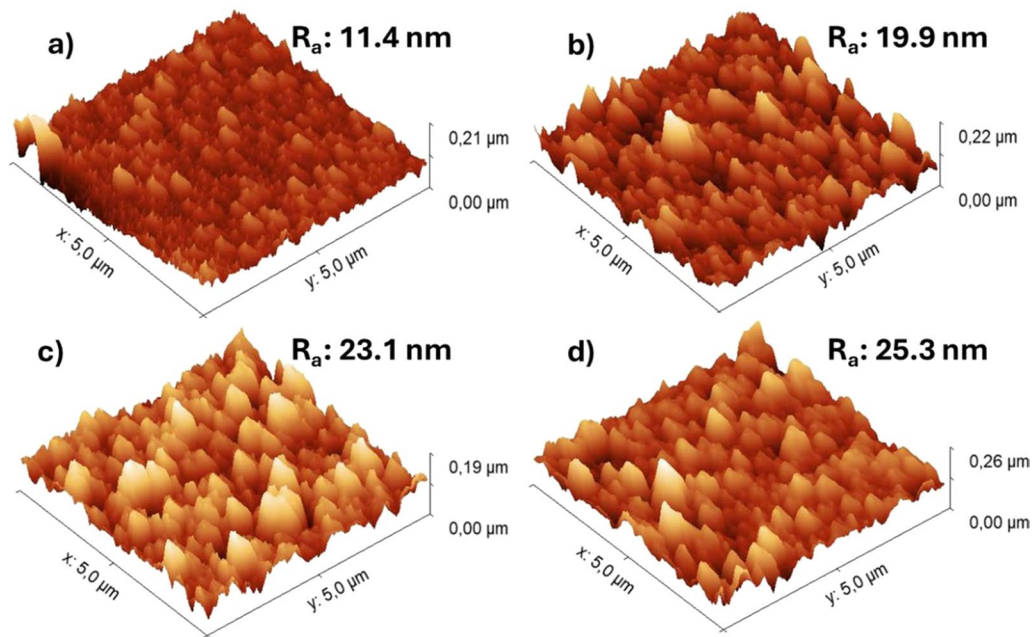


Fig. 5 3D AFM images of the Cu₂O thin films deposited at (a) 20, (b) 40, (c) 60, and (d) 80 cycles.

The surface roughness determined from the $5 \times 5 \mu\text{m}^2$ AFM images was 11.4 nm, 19.9 nm, 23.1 nm, and 25.3 nm for the Cu_2O thin films deposited at 20, 40, 60, and 80 cycles, respectively.

The surface energy characteristics of the Cu_2O thin films were also analyzed from contact angle measurements, employing water and ethylene glycol as testing liquids. The surface energy is the energy associated with intermolecular forces at the interface between two media and provides important information about the capability of the thin film surface to interact with the surrounding liquids or gases. Figure 6a shows the water and ethylene glycol contact angles measured on the surface of the Cu_2O thin films, and Fig. 6b their corresponding surface energy, as a function of the number of cycles. The contact angle for both testing liquids displays some variations with the number of cycles, which can be due to the observed changes in the surface roughness of the thin films. The water contact angle values between 60° and 70° reveal that the Cu_2O thin film surface is rather

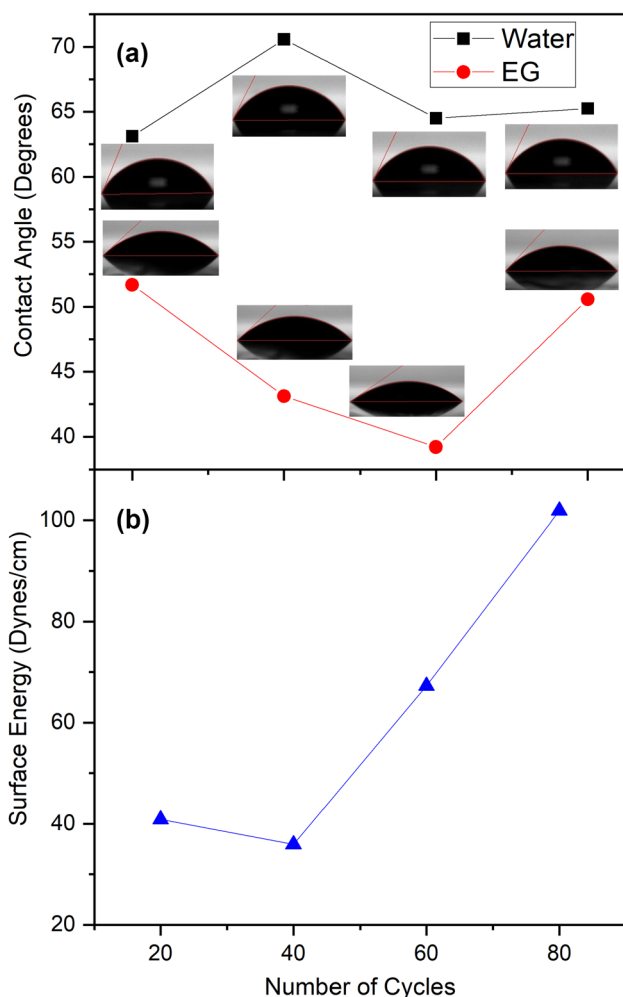


Fig. 6 (a) Contact angle and (b) surface energy versus number of cycles of the Cu_2O thin films.

hydrophobic, while the values for ethylene glycol between 40° and 50° mark a tendency to its oleophilicity. These characteristics of Cu_2O have been reinforced in core-shell hybrid nanofibers of Cu_2O -PMMA with super hydrophobicity and oleophilicity, which were applied successfully in the separation of oil from water. On the other hand, the surface energy of the Cu_2O thin films shows an increasing trend with the number of cycles, like the behavior of the surface roughness. This is because surface roughness influences the surface energy of a solid. In generally, increased surface roughness enhances their surface energy because a rough material has a larger total surface area than a smooth material due to the tiny depressions and thus offers a larger wetting area.

Figure 7 shows the optical transmittance (T) and reflectance (R) spectra of the complete set of Cu_2O thin films, and for comparison, the corresponding optical spectra of the glass substrate. The transmittance of the thin films at wavelengths higher than 550 nm is constant in the range of 80–90% depending on the number of cycles. The thicker films are less transparent in this region. At lower wavelengths, the transmission of the thin films decreases, indicating that the absorption edge of the Cu_2O thin films is around the wavelength of 550 nm. In this region, it is observed that the thicker the Cu_2O thin films, the higher the optical transmission reduction. On the other hand, the optical reflection of the thin films at higher wavelengths is in the 7–13% range, increasing with the thickness of the films. The absorption edge can be seen better in the spectrum of the thickest film deposited at 80 cycles. The absorption coefficient, $\alpha(\lambda)$,

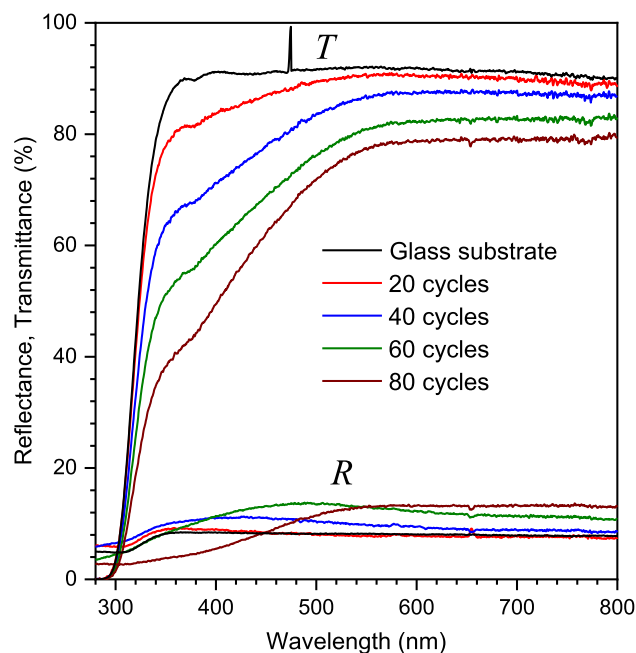


Fig. 7 Transmittance (T) and reflectance (R) optical spectra of the Cu_2O thin films deposited at 20, 40, 60, and 80 cycles.

spectra of the Cu₂O thin films were determined from their T spectra employing the following equation:

$$\alpha(\lambda) = \frac{1}{t} \ln \left[\frac{1}{T} \right] \quad (7)$$

where t is the thickness of the thin films. Then, by using the Tauc relation,

$$ah\nu = A(h\nu - E_g)^n \quad (8)$$

where $h\nu$ is the photon energy, A is a constant, and E_g is the energy bandgap, with $n=1/2$, which corresponds to allowed direct transitions, the $(\alpha h\nu)^{1/2}$ spectra were plotted and fitted in the linear region to calculate the energy bandgap of the Cu₂O thin films. The results are shown in Fig. 8, where the dashed straight lines represent the best linear fits of Eq. (8) to the experimental data. The E_g values for the different films, determined from the intersection of these dashed lines with the energy axis, are included as insets in the Tauc plots. The values of E_g versus film thickness do not exhibit a trend, only a lower value of 2.43 eV for the film deposited at 20 cycles, which may be due to the lack of a sharp absorption

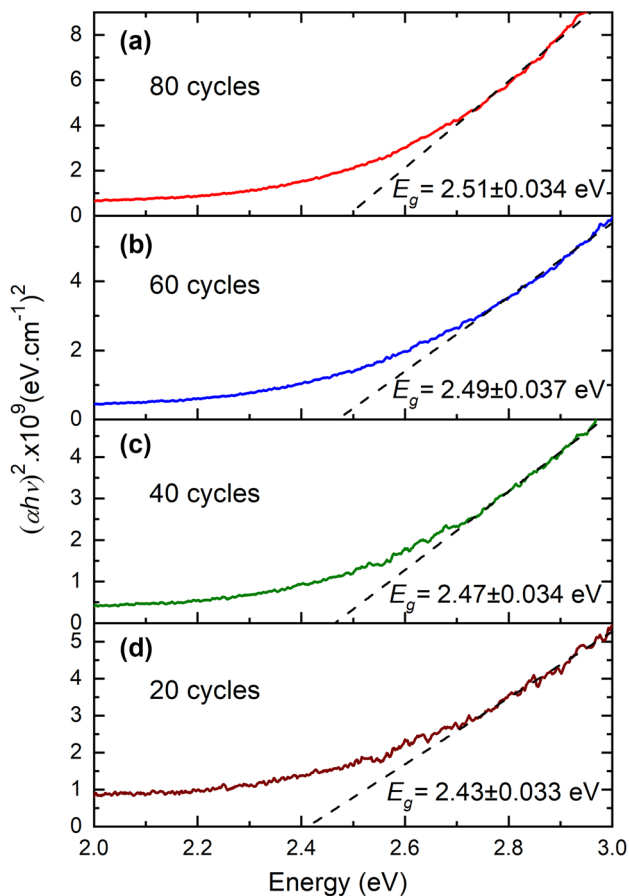


Fig. 8 Tauc plots for determining the energy bandgap of the Cu₂O thin films deposited at (a) 80, (b) 60, (c) 40, and (d) 20 cycles.

edge in the spectrum of this film. These values are in the range of the energy bandgap reported for thin films with the Cu₂O crystalline phase.^{9,40} Although these values are rather high, they are in agreement with the energy bandgap reported for Cu₂O thin films obtained by SILAR with copper acetate as the copper precursor, whose value is 2.47 eV.²⁶ Among the different reasons to explain the high values of the energy bandgap of Cu₂O thin films, the most commonly reported explanation is quantum size effects, which can be significant in direct-bandgap semiconductors. The nanoscale structure of Cu₂O with small particle size can increase its energy bandgap, as reported in the literature. For example, chemically deposited Cu₂O thin films with an energy bandgap of 2.44 eV were reported by Ahirrao et al.,⁴¹ who attributed the high energy bandgap value to the decrease of the particle size.⁴¹ Also, employing the same CBD technique, Xu et al. reported high energy bandgap values in the range of 2.49–2.7 eV, attributed also to the effects of quantum confinement.²¹

The electrical resistivity of the Cu₂O thin film deposited at 80 cycles was determined from the transmission line methods, by measuring the current versus voltage (I – V) curves at different distances, L , between coplanar electrodes. These measurements are shown in the inset of Fig. 9, where the linear behavior reveals the ohmic characteristics of the contacts. The slope of these straight lines decreases with the distance between the electrodes due to the increase of the

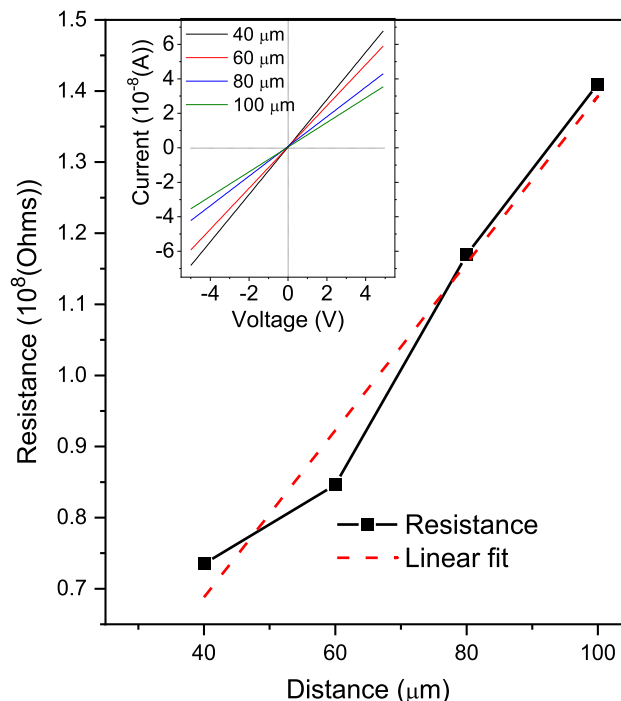


Fig. 9 Electrical resistance versus distance between electrodes measured in the Cu₂O thin film deposited at 80 cycles. The inset displays the I – V curves measured at the different distances between electrodes.

electrical resistance, whose values are plotted as a function of L in this figure. The dashed line in this graph represents the best linear fit to the experimental data, which is substituted in the following equation to determine the electrical resistivity, ρ , of the Cu_2O thin film:

$$R(L) = R_C + \rho \frac{L}{A} \quad (9)$$

where A is the area of the transverse section of the thin film, and R_C is the resistance of the contacts, which is obtained by the intersection of the straight line at $L = 0$, $R(0) = R_C$. The results obtained for the electrical resistivity and contact resistance for this Cu_2O thin film were $3.55 \times 10^3 \, \Omega \text{ cm}$ and $2.18 \times 10^7 \, \Omega \text{ cm}$, respectively. The electrical resistivity reported for Cu_2O thin films depends on the deposition and post-deposition annealing temperatures. For example, in the work by Ozaslan et al., Cu_2O thin films were deposited by the SILAR technique at a temperature of 70°C and subsequently thermally annealed in air at temperatures of 100°C , 300°C , and 500°C . The value of the electrical resistivity of the as-deposited Cu_2O thin film (70°C) was $6.12 \times 10^4 \, \Omega \text{ cm}$, while those films annealed at 100°C , 300°C , and 500°C had electrical resistivity values of $7.44 \times 10^3 \, \Omega \text{ cm}$, $8.23 \times 10^3 \, \Omega \text{ cm}$, and $5.11 \times 10^2 \, \Omega \text{ cm}$, respectively. The crystalline structure of these annealed thin films changed to the CuO crystalline phase at a temperature of 300°C , which together with their densification into a more closely packed microstructure produced the observed modifications to the electrical resistivity.⁴² Table I shows the electrical resistivity of Cu_2O thin films deposited by SILAR and other techniques reported in the literature. These values confirm the influence of the deposition temperature and the temperature of post-deposition treatments. As can be seen, the values of electrical resistivity of the Cu_2O thin films deposited by SILAR are in the range of 10^2 – $10^4 \, \Omega \text{ cm}$. Therefore, the electrical resistivity of our Cu_2O thin films deposited at room temperature lies in the range of values reported in the literature included in this table.

Rapid thermal annealing (RTA) at 200 and 250° was carried out on the Cu_2O thin film deposited at 80 cycles for 1 min, 3 min, and 5 min. The XRD patterns of the annealed thin films at 200°C and 250°C are presented in Fig. 10a and b, respectively. The diffraction peaks for the cubic Cu_2O (PDF #05-0667) and cubic Cu (PDF #04-0836) crystalline phases are included at the bottom and the top, respectively. The observed peaks in these patterns at 36.48° , 42.36° , 61.36° , and 73.58° match with the (111), (200), (220), and (311) diffraction lines characteristics of the Cu_2O crystalline phase, respectively. For both annealing temperatures, the intensity of the diffraction peaks increases with annealing time, indicating the enhancement of the Cu_2O thin film crystallinity. However, the pattern of the Cu_2O thin film annealed at 250°C for 5 min displays weak signals at 43.25° and 50.5° related to the (111) and (200) crystalline planes of the metallic Cu phase, respectively. Therefore, the RTA at 250°C produces some reduction effects on the Cu_2O thin films, which results in the formation of the metallic Cu phase. The crystal size, D , of the Cu_2O phase was calculated from these patterns by using the well-known Scherrer formula:

$$D = \frac{0.9\lambda}{\beta \cos\theta} \quad (10)$$

where λ is the x-ray wavelength, β is the full width at half maximum (FWHM) of the diffraction peak, and θ is the Bragg angle. For this, the (111) diffraction peaks were fitted to Gaussian functions to determine their FWHM. The results are shown in Table II, where an increase in crystal size with time and temperature of the RTA treatment is observed.

Figure 11 shows the HR-XPS spectra in the $\text{Cu } 2p$ region of the Cu_2O thin films after rapid thermal annealing at 250°C for 1 min, 3 min, and 5 min. The two peaks observed at binding energies of 942 eV and 944 eV have been assigned to the spin-orbit pair of $\text{Cu } 2p_{3/2}$ and $\text{Cu } 2p_{1/2}$ of Cu^+ , respectively, which is consistent with the formation of the Cu_2O phase.^{22,45,46} However, the deconvolution of the HR-XPS spectra in the $\text{Cu } 2p_{3/2}$ region, shown in

Table I Electrical resistivity of Cu_2O thin films deposited by SILAR and other techniques

Deposition technique	Temperature ($^\circ\text{C}$)	Resistivity ($\Omega \text{ cm}$)	References
SILAR	70 (as-deposited)	6.12×10^4	42
	100 (thermal treatment)	7.44×10^3	
	70 (as-deposited)	$(1.8\text{--}3.73) \times 10^2$	27
	60 (as-deposited)	1.24×10^4	26
	Room temperature	3.55×10^3	This work
	250 (thermal treatment)	1.33×10^2	
Dip-coating	200 (thermal treatment)	4.71×10^3	36
	400 (thermal treatment)	9.9×10^1	43
RF sputtering	Room temperature	1×10^4	44
CBD	Room temperature	1.2×10^3	41

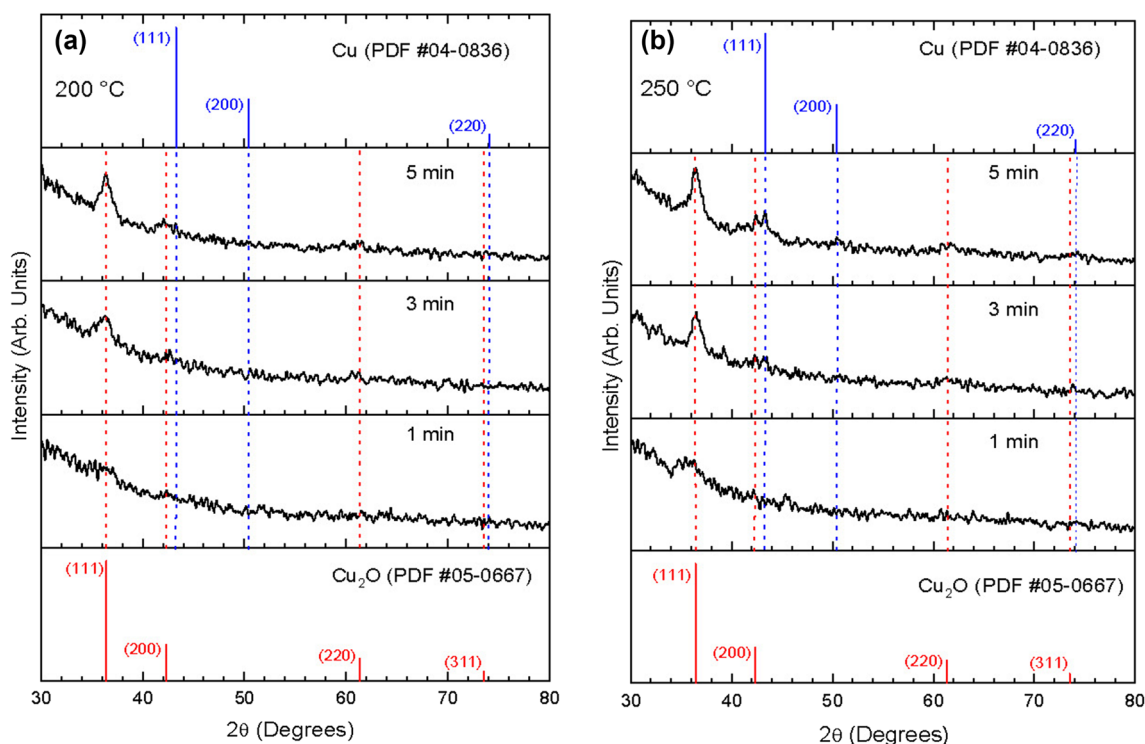


Fig. 10 XRD patterns of the Cu₂O thin films with RTA for 1 min, 3 min, and 5 min at (a) 200°C and (b) 250°C.

Table II Crystal size of the Cu₂O thin films with RTA for 1 min, 3 min, and 5 min at 200°C and 250°C

1 min		3 min		5 min	
200°C	250°C	200°C	250°C	200°C	250°C
<i>D</i> (nm)	<i>D</i> (nm)	<i>D</i> (nm)	<i>D</i> (nm)	<i>D</i> (nm)	<i>D</i> (nm)
–	3.6	3.7	8.6	6.4	7.3

Fig. 12a, where the XPS signals were deconvoluted using four singlet peaks with a Voigt profile, reveals the presence of both Cu¹⁺ and Cu²⁺ oxidation states. These chemical components are related to the XPS peaks located at around 933 eV and 935 eV, respectively.⁴⁶ Furthermore, the weaker peaks centered at 942 eV and 944 eV correspond to satellite peaks characteristic of the oxidation state Cu²⁺.⁴⁶ These results show the formation of an amount of the CuO phase. Nevertheless, this phase was not observed in the XRD patterns. This discrepancy is explained in terms of the surface sensitivity of the XPS technique of around 5–10 nm, as compared to the XRD technique, in which the penetration depth can be up to 20 microns. Therefore, it can be assumed that the CuO phase is formed on the surface of the Cu₂O thin film as a consequence of slight oxidation upon contact with the environment.^{46,47} The Cu¹⁺/Cu²⁺ area ratio was obtained by comparing the total intensity of peaks of Cu¹⁺ and Cu²⁺, where the total area of Cu²⁺ includes the

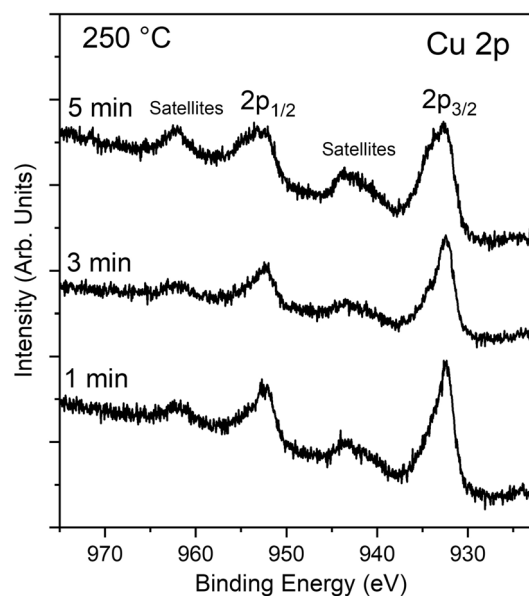


Fig. 11 XPS spectra in the Cu 2p region of the of the Cu₂O thin films with RTA for 1 min, 3 min, and 5 min at 250°C.

satellite peaks. The values shown in Table III were 1.69 (1 min), 1.98 (3 min), and 0.98 (5 min). Interestingly, the Cu²⁺ oxidation state decreases from an annealing time of 1 min to 3 min, while this component increases again for an annealing time of 5 min. This result demonstrates that

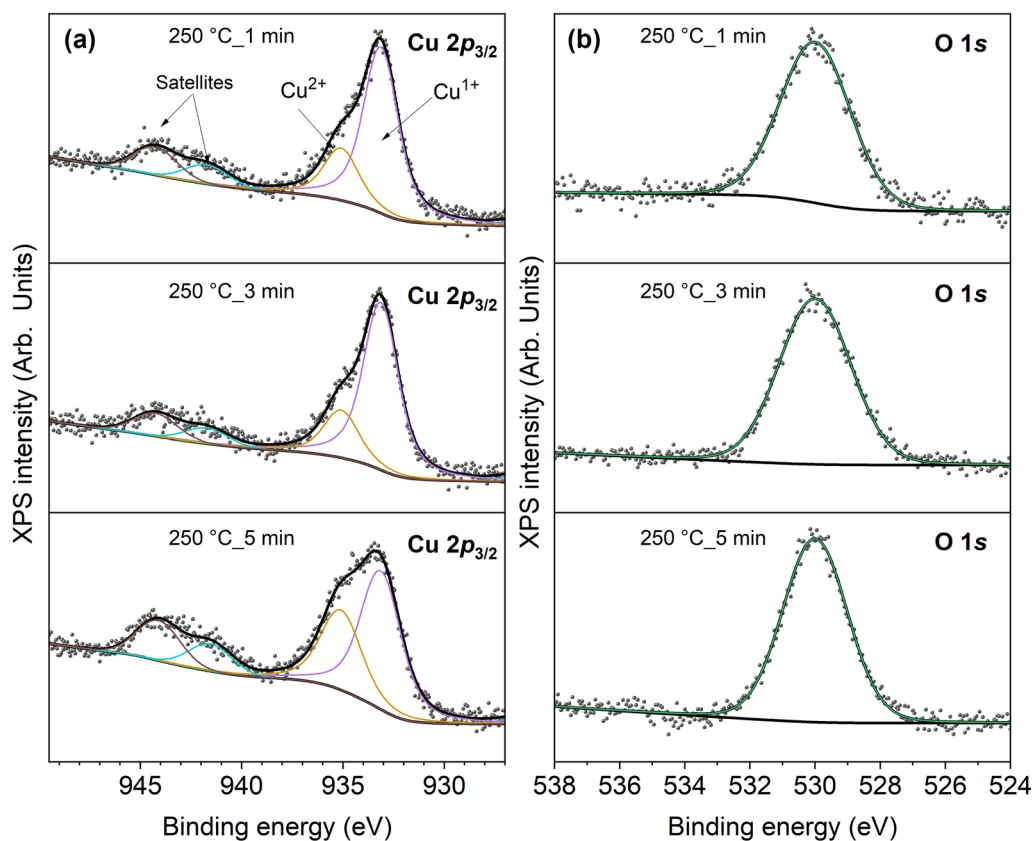


Fig. 12 XPS spectra in the (a) Cu $2p_{3/2}$ and (b) O $1s$ regions of the of the Cu_2O thin films with RTA for 1, 3, and 5 min at 250°C .

Table III Cu^{1+} , Cu^{2+} , and $\text{Cu}^{1+}/\text{Cu}^{2+}$ area ratio of the Cu_2O thin films with RTA for 1 min, 3 min, and 5 min at 250°C , determined from the fittings to the XPS spectra in the Cu $2p_{3/2}$ region

RTA (min)	Cu^{1+} (%)	Cu^{2+} (%)	$\text{Cu}^{1+}/\text{Cu}^{2+}$
1	62.8	37.2	1.69
3	66.4	33.6	1.98
5	49.5	50.5	0.98

the RTA treatments produced reduction effects on the Cu_2O thin films, as observed in the XRD patterns. On the other hand, at the right in Fig. 12b, the O $1s$ signal of the Cu_2O thin films was fitted using a single peak located at 530 eV. This chemical component is associated with Cu–O bonds.⁴⁸

The surface morphological characteristics of the Cu_2O thin films subjected to RTA were analyzed using SEM images shown in Fig. 13. The images in Fig. 13a, b, and c correspond to the films annealed at 200°C for 1 min, 3 min, and 5 min, respectively, while the images in Fig. 13d, e, and f correspond to the samples annealed at 250°C for 1 min, 3 min, and 5 min, respectively. The RTA at 200°C does not produce a significant change in the morphology of the Cu_2O thin films, which retain their compact granular and

homogeneous surface. On the other hand, the RTA at 250°C resulted in a thin film surface with more compact grains and some protruding agglomerations, observed mainly after 3 min.

Figure 14 displays the T and R optical spectra of the Cu_2O thin films after the RTA at (a) 200°C and (b) 250°C . The corresponding spectra of the thin film before RTA are included for comparison. At both annealing temperatures, a shift to higher wavelength of the absorption edge of the Cu_2O thin films is observed. The longer the RTA time, the higher the red shift of the absorption edge, indicating a reduction in the energy bandgap of the annealed Cu_2O thin films. In addition, the optical reflectance is increased to values around 30% of the thin film annealed at 250°C for 5 min, which could be due to the metallic Cu phase formed in this sample. Similar to the as-deposited Cu_2O thin films, the energy bandgaps of the thin films after the RTA were determined from the Tauc plots shown in Fig. 15a and b for temperatures of 200°C and 250°C , respectively. In this graph, the dashed lines represent the best fit to the theoretical model, where the intersection with the energy axis provides the energy bandgap value in each case. In both cases, the value of the energy bandgap decreases slightly with the time of RTA from 2.51 eV to 2.36–2.42 eV. At a temperature of 200°C , the RTA treatment

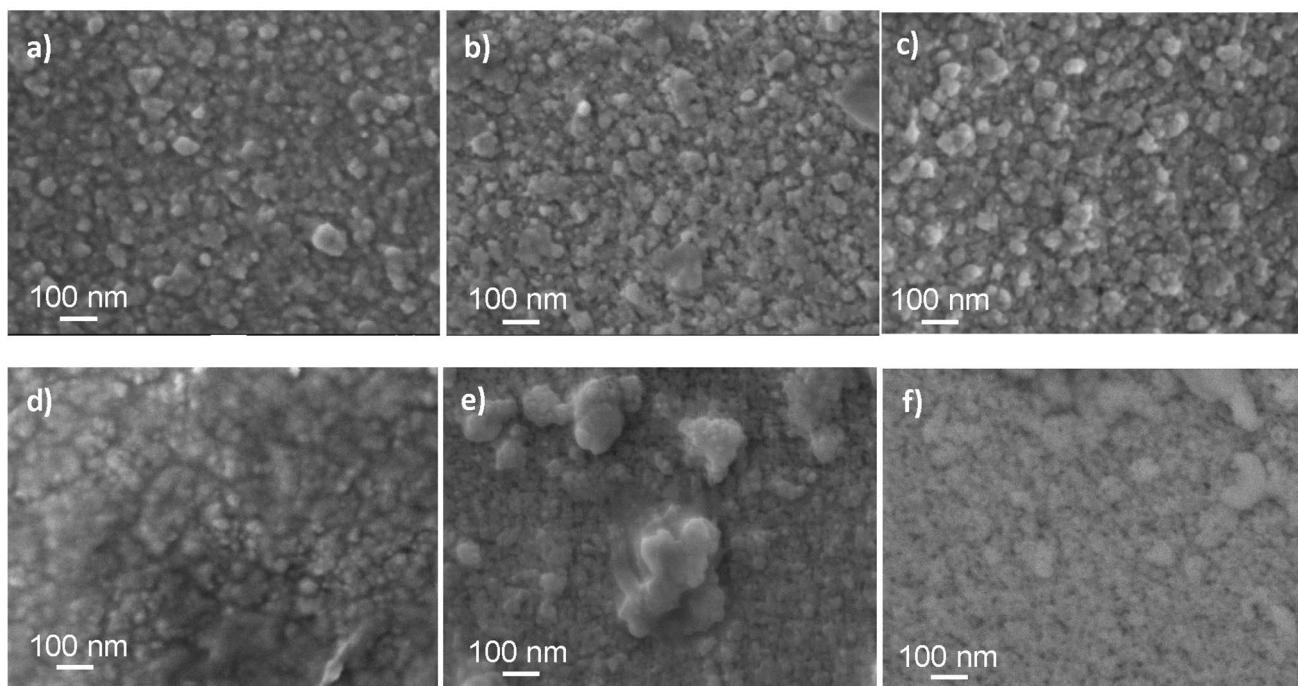


Fig. 13 SEM images of the Cu₂O thin film heat-treated by RTA at 200°C for (a) 1 min, (b) 3 min, and (c) 5 min and 250°C for (d) 1 min, (e) 3 min, and (f) 5 min.

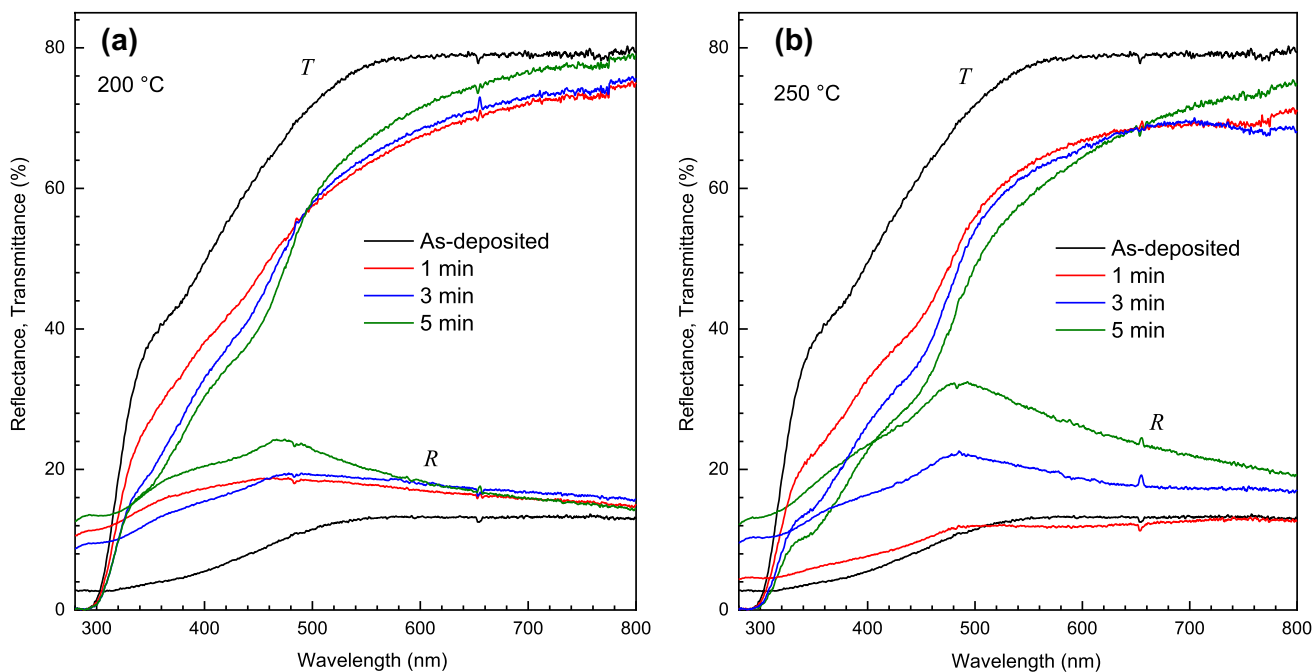


Fig. 14 Transmittance (*T*) and reflectance (*R*) optical spectra of the Cu₂O thin films with RTA for 1 min, 3 min, and 5 min at (a) 200°C, and (b) 250°C.

resulted in a reduction of the energy bandgap of the Cu₂O thin films to values in the range of 2.42–2.45 eV depending on the treatment time. On the other hand, at 250°C,

there is also a reduction of the energy band gap after 1 min (2.38 eV) and 3 min (2.36 eV) treatment, which is followed by an increase after 5 min (2.39 eV). The energy bandgap

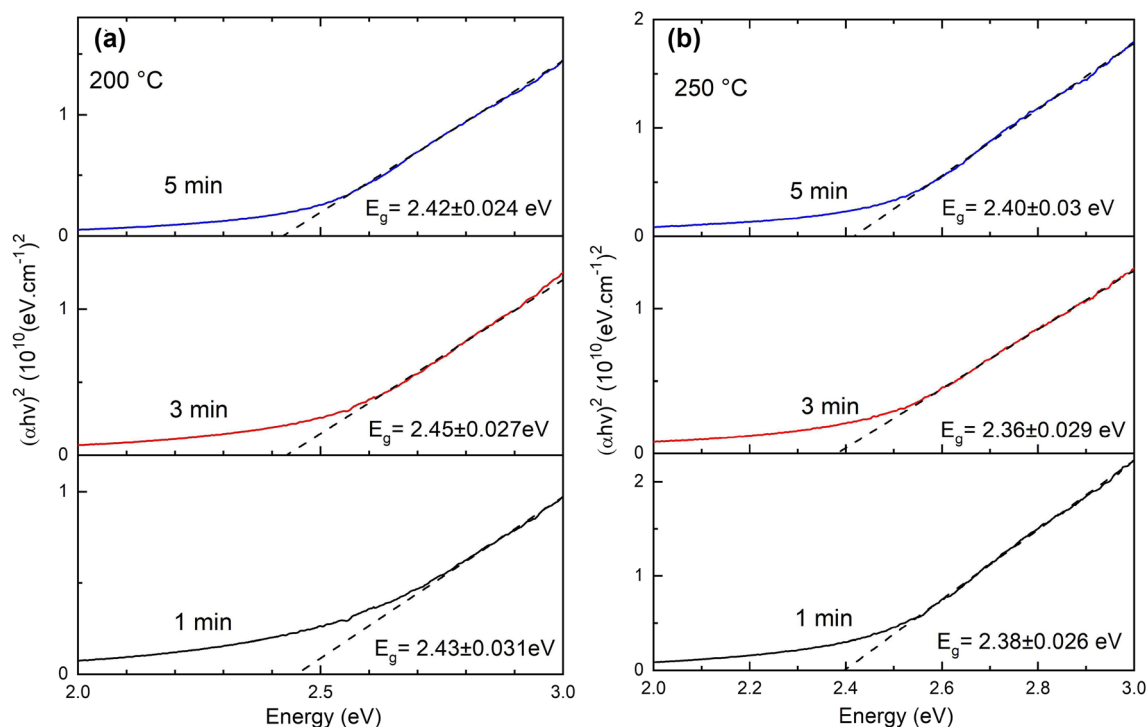


Fig. 15 Tauc plots for determining the energy bandgap of the Cu_2O thin films with RTA for 1 min, 3 min, and 5 min at (a) 200 and (b) 250°C.

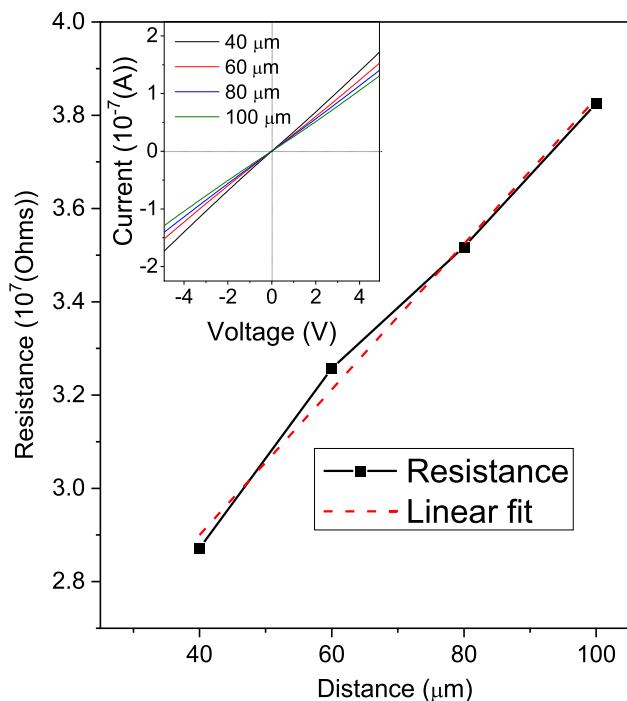


Fig. 16 Electrical resistance versus distance between electrodes measured in the Cu_2O thin film deposited at 80 cycles. The inset displays the I - V curves measured at the different distances between electrodes.

behavior of the annealed films at 250°C could be due to the presence of the Cu phase in the composition of the thin films. The energy bandgap value reported for Cu_2O thin films obtained after RTA treatment at 400°C is 2.36 eV,⁴³ which is quite close to the values reported here. In general, the wide range of energy bandgap values reported for Cu_2O thin films reflects their different characteristics, such as crystal size, thickness, and doping.⁴⁹ As mentioned above, the most common reason for obtaining Cu_2O thin films with high energy bandgap values is quantum confinement effects due to their small crystal size, on the order of 2–14 nm.^{50–52} This is because the Bohr exciton radius of Cu_2O is 2.5 nm,⁵³ and then when the crystal size of Cu_2O thin films is close to this critical radius, quantum confinement effects result in an increase in the energy bandgap values. According to the XRD analysis of the Cu_2O thin films with RTA at 250°C, their crystal sizes are in the range of 3.6–8.6 nm, close to the critical radius for quantum confinement effects, which can explain the high values of the energy bandgap of these films.

The electrical resistivity of the Cu_2O thin film deposited at 80 cycles after RTA was also determined from the transmission line method, and the results are shown in Fig. 16, where the inset displays the current versus voltage (I - V) curves measured at the different values of L . The values of the resistance versus L decreases around one order of magnitude, and the observed current increases in the same proportion, as compared to the measured values

Table IV Electrical resistivity of the Cu₂O thin films after RTA at 200 and 250°C for 1 min, 3 min, and 5 min

1 min		3 min		5 min	
200°C	250°C	200°C	250°C	200°C	250°C
ρ 10 ³ Ω cm)	ρ 10 ² (Ω cm)	ρ 10 ² (Ω cm)	ρ 10 ² (Ω cm)	ρ 10 ² (Ω cm)	ρ 10 ² (Ω cm)
6.36	2.55	3.25	1.33	5.21	3.41

before the RTA process (Fig. 9). Table IV shows the electrical resistivity values of the Cu₂O thin films as a function of the RTA time for both temperatures, 200°C and 250°C. The thin film treated at 200°C for 1 min has an electrical resistivity on the order of 10³ Ω cm, the same order as the as-deposited thin film. However, after 3 min and 5 min of RTA treatment, the resistivity of these thin films decreases one order of magnitude to 10² Ω cm. On the other hand, the values of the contact resistance of the samples annealed with RTA were in the same order of 10⁷ Ω cm as that of the sample without RTA. The reduction of one order of magnitude of the resistivity of the RTA-treated thin films is also observed at the temperature of 250°C. The lowest resistivity of 1.33 × 10² Ω cm was determined for the thin film treated at 250°C for 3 min. Furthermore, for both temperatures, we can observe a slight increase in the resistivity from 3 min to 5 min of RTA treatment. This feature can be also due to the formation of metallic copper aggregates in the Cu₂O thin films, which can function as charge dispersion centers.⁴³ Khoo et al. reported this trend when the temperature increases in an RTA process; the electrical resistivity decreases for Cu₂O layers in a chemically electrodeposited *n*-ZnO/*p*-Cu₂O photovoltaic device, obtaining a minimum value of 3.1 × 10⁴ Ω cm at 523 K. The authors conclude that as the treatment temperature increases, the number and size of pores increase, while the grain boundaries in the thin films decrease.⁵⁴ An efficient heat treatment such as RTA improves the electrical properties of Cu₂O films, as in this case, where the lowest value of the electrical resistivity is on the order of 10² Ω cm, which is consistent with the values reported in other works using this type of RTA treatments.^{55,56} Regarding the influence on the electrical resistivity of the metallic Cu observed by XRD in the films treated at 250°C, we assume that it is negligible for two reasons. According to the relative intensity of the (111) Cu diffraction peak in the XRD patterns of Fig. 10b, the amount of Cu phase in the films treated at 250°C for 3 min and 5 min should not be enough to form conductive paths between electrodes. The resistivity of these films on the order of 10² Ω cm is consistent with this. Furthermore, based again on the XRD analysis, the amount of Cu phase in the film treated at 250°C for 5 min is higher; however,

the electrical resistivity of this film decreases as compared to that of the film treated for 3 min, instead of increasing as expected if the Cu phase had influence.

Conclusions

In this work we reported a two-step ammonia-free SILAR process for the deposition of thin films of copper oxide(I) (Cu₂O) at room temperature, employing low-toxicity precursors at low concentrations and an ammonia-free complexing agent. It was possible to optimize this deposition technique to minimize the number of steps, assuring the good quality of the Cu₂O thin films. These thin films were polycrystalline with the cubic crystalline phase of Cu₂O, with thickness and energy bandgap values in the 30–120 nm and 2.43–2.51 eV ranges, respectively, depending on the number of cycles during deposition. In addition, the electrical resistivity of the thickest Cu₂O thin film was on the order of 10³ Ω cm. When subjected to RTA treatments, the Cu₂O thin films increased their crystal size, from 3.6 nm to 8.6 nm, with a reduction in the electrical resistivity by one order of magnitude, and in the energy bandgap to values of 2.38 eV. The surface morphology of the treated thin films became more compact, which was corroborated by SEM images. The XRD analysis showed the increase of the crystal size with time and temperature of the RTA, resulting in values in the range of 3.6–8.6 nm, close to 2.5 nm, which is the Bohr exciton radius of Cu₂O. However, XPS analysis revealed the presence of the CuO phase on the surface of the RTA-treated Cu₂O thin films, and XRD showed the presence of small amounts of the metallic copper phase after 5 min of RTA at 250°C. The minimum values of energy bandgap and electrical resistivity were 2.38 eV and 133 Ω cm, respectively, and were achieved for the Cu₂O thin film after RTA treatment of 3 min. Despite challenges such as the presence of CuO and metallic copper phases, our findings demonstrated that the ammonia-free SILAR process enables the deposition of polycrystalline Cu₂O thin films at room temperature, providing valuable insights for the further development of this promising semiconductor material in several optoelectronic applications.

Acknowledgments The helpful technical support of Carlos Alberto Avila Herrera, Martín Adelaido Rodríguez, Araceli Mauricio Sánchez, and Eleazar Urbina Alvarez is gratefully acknowledged.

Funding The authors declare that no funds, grants, or other support were received during the preparation of this manuscript. The authors have no relevant financial or non-financial interests to disclose.

Conflict of interest The authors declare that they have no conflict of interest.

Open Access This article is licensed under a Creative Commons Attribution 4.0 International License, which permits use, sharing, adaptation, distribution and reproduction in any medium or format, as long as you give appropriate credit to the original author(s) and the source, provide a link to the Creative Commons licence, and indicate if changes were made. The images or other third party material in this article are included in the article's Creative Commons licence, unless indicated otherwise in a credit line to the material. If material is not included in the article's Creative Commons licence and your intended use is not permitted by statutory regulation or exceeds the permitted use, you will need to obtain permission directly from the copyright holder. To view a copy of this licence, visit <http://creativecommons.org/licenses/by/4.0/>.

References

- H. He, *Solution processed metal oxide thin films for electronic applications* (New York: Elsevier, 2020), p.7.
- A. Pierre and A.C. Arias, Solution-processed image sensors on flexible substrates. *Flex. Print. Electron.* 1, 043001 (2016).
- F. Xue, L. Chen, J. Chen, J. Liu, L. Wang, M. Chen, Y. Pang, X. Yang, G. Gao, J. Zhai and Z. Wang, P-type MoS₂ and n-type ZnO diode and Its performance enhancement by the piezophototronic effect. *Adv. Mater.* 28, 3391 (2016).
- X. Chen, G. Liu, Y. Hu, W. Cao, P. Hu, and W. Hu, Vertical MoSe₂-MoO_x p-n heterojunction and its application in optoelectronics. *Nanotechnology* 29, 045202 (2018).
- T. Ji, Y. Cao, X. Peng, Y. Zhang, L. Sun, L. Wang, R. Zou, Y. Sivalingam, W. Han, and J. Hu, A facile method to fabricated UV-Vis photodetectors based on TiO₂/Si heterojunction. *Appl. Surf. Sci.* 449, 358 (2018).
- D.Y. Kim, J. Ryu, J. Manders, J. Lee, and F. So, Air-stable, solution-processed oxide p-n heterojunction ultraviolet Photodetector. *ACS Appl. Mater. Interfaces* 6, 1370 (2014).
- D. Zhang, C. Liu, R. Xu, B. Yin, Y. Chen, X. Zhang, F. Gao, and S. Ruan, The effect of self-depleting in UV photodetector based on simultaneously fabricated TiO₂/NiO pn heterojunction and Ni/Au composite electrode. *Nanotechnology* 28, 365505 (2017).
- B.K. Meyer, A. Polity, D. Reppin, M. Becker, P. Hering, B. Kramm, P. Klar, T. Sander, C. Reindl, C. Heiliger, M. Heineemann, C. Muller, and C. Ronning, The physics of copper oxide (Cu₂O). *Semicond. Semimet.* 88, 201 (2013).
- D.S. Murali, S. Kumar, R.J. Choudhary, A.D. Wadikar, M.K. Jain, and A. Subrahmanyam, Synthesis of Cu₂O from CuO thin films: optical and electrical properties. *AIP Adv.* 5, 1 (2015). <https://doi.org/10.1063/1.4919323>.
- R.K. Gupta, K. Ghosh, and P.K. Kahol, Effect of temperature on current-voltage characteristics of Cu₂O/p-Si Schottky diode. *Phys. E* 41, 876 (2009).
- M. Abdelfatah, W. Ismail, and A. El-Shaer, Low cost inorganic white light emitting diode based on submicron ZnO rod arrays and electrodeposited Cu₂O thin film. *Mater. Sci. Semicond. Process.* 81, 44 (2018).
- K. Han and M. Tao, Electrochemically deposited p-n homojunction cuprous oxide solar cells. *Sol. Energy Mater. Sol. Cells* 93, 153 (2009).
- J. Jang, S. Chung, H. Kang, and V. Subramanian, P-type CuO and Cu₂O transistors derived from a sol-gel copper (II) acetate monohydrate precursor. *Thin Solid Films* 600, 157 (2016).
- S. Dolai, S. Das, S. Hussain, R. Bhar and A.K. Pal, Cuprous oxide (Cu₂O) thin films prepared by reactive d.c. sputtering technique. *Vacuum* 141, 296 (2017).
- R. Bunea, A.K. Saikumar, and K. Sundaram, The effect of annealing temperature and reactive gases on optical properties of Cu₂O thin films. *Mater. Sci. Appl.* 12, 182 (2021).
- A. El Kasmi, Z.Y. Tian, H. Vieker, A. Beyer, and T. Chafik, Innovative CVD synthesis of Cu₂O catalysts for CO oxidation. *Appl. Catal. B Environ.* 186, 10 (2016).
- D. Dai, P.Y. Huang, T.Y. Wu, C.H. Shih, and L. Chang, Epitaxial electrodeposition of Cu₂O on Ag substrates in sulfate baths. *J. Cryst. Growth* 603, 126983 (2023).
- D. Osorio-Rivera, G. Torres-Delgado, R. Castanedo-Pérez, J. Márquez-Marín, and O. Zelaya-Ángel, Cd₂SnO₄/CdS/Cu₂O/Ag solar cell obtained by chemical techniques. *Mater. Res. Bull.* 122, 110669 (2020).
- P.S. Mandlik, A.S. Landge, M.A. Ingole, and S.V. Bhosale, Synthesis of highly superhydrophilic Cu₂O film using dip coating method. *Mater. Today Proc.* 84, 1 (2023).
- H.Y. Xu, C. Chen, L. Xu, and J.K. Dong, Direct growth and shape control of Cu₂O film via one-step chemical bath deposition. *Thin Solid Films* 527, 76 (2013).
- H. Xu, J. Dong, and C. Chen, One-step chemical bath deposition and photocatalytic activity of Cu₂O thin films with orientation and size controlled by a chelating agent. *Mater. Chem. Phys.* 143, 713 (2014).
- S. Chatterjee, S.K. Saha, and A.J. Pal, Formation of all-oxide solar cells in atmospheric condition based on Cu₂O thin-films grown through SILAR technique. *Sol. Energy Mater. Sol. Cells* 147, 17 (2016).
- K. Dhanabalan, A.T. Ravichandran, K. Ravichandran, S. Valanarasu, and S. Mantha, Effect of Co doped material on the structural, optical and magnetic properties of Cu₂O thin films by SILAR technique. *J. Mater. Sci. Mater. Electron.* 28, 4431 (2017).
- D. Ozaslan, O.M. Ozkendir, M. Gunes, Y. Ufuktepe, and C. Gumus, Study of the electronic properties of Cu₂O thin films by X-ray absorption spectroscopy. *Optik* 157, 1325 (2018).
- F. Baig, Y.H. Khattak, B.M. Soucase, S. Beg, and S. Ullah, Effect of anionic bath temperature on morphology and photo electrochemical properties of Cu₂O deposited by SILAR. *Mater. Sci. Semicond. Process.* 88, 35 (2018).
- G. Altindemir, and C. Gumus, Cu₂O thin films prepared by using four different copper salts at a low temperature: an investigation of their physical properties. *Mater. Sci. Semicond. Process.* 107, 104805 (2020).
- S.F.U. Farhad, M.A. Hossain, N.I. Tanvir, R. Akter, M.A.M. Patwary, M. Shahjahan, and M.A. Rahman, Structural, optical, electrical, and photoelectrochemical properties of cuprous oxide thin films grown by modified SILAR method. *Mater. Sci. Semicond. Process.* 95, 68 (2019).
- H. Soonmin, Recent advances in the growth and characterizations of SILAR-deposited thin films. *Appl. Sci.* 12, 1 (2022).
- M.A.M. Patwary, M.A. Hossain, B.C. Ghos, J. Chakrabarty, S.R. Haque, S.A. Rupa, J. Uddin, and T. Tanaka, Copper oxide nanostructured thin films processed by SILAR for optoelectronic applications. *RSC Adv.* 12, 32853 (2022).
- A. Vasuhi, K. Dhanabalan, A.T. Ravichandran, R. Chandramohan, and S. Mantha, Enhancement of structural, optical and bumpy surface effect of Cu₂O thin films through Sn doping by modified SILAR technique. *Int. J. Thin Film Sci. Technol.* 11, 327 (2022).
- A. Vasuhi, K. Dhanabalan, A. Ravichandran, R. Chandramohan, K. Ravichandran, R. Shalini, and S. Mantha, Influence of effective surface area on gas sensing properties and surface morphology of Ag doped Cu₂O thin films by cost effective method of M-SILAR technique. *Int. J. Thin Film Sci. Technol.* 12, 181 (2023).
- S. Sassi, K. Trabelsi, A. El Jery, M. Abidi, A. Hajjaji, L. Khezami, A. Karrech, M. Gaidi, B. Soucase, and B. Bessais, Synergistic effect of Cu_xO_y-NPs/TiO₂-NTs heterostructure on the photodegradation of amido black staining. *Optik* 272, 170234 (2023).

33. T.T. Lun, C.Q. Liu, N. Wang, X.N. Zhai, M.S. Song, Q. Ge, X.Y. Zhang, and S.M. Liu, Preparation of compact CuO films by sol-gel spin coating technique. *Mater. Lett.* 257, 1 (2019).
34. T. Çayır Taşdemirci, Copper oxide thin films synthesized by SILAR: role of varying annealing temperature. *Electron. Mater. Lett.* 16, 239 (2020).
35. M. Abdel Rafea, and N. Roushdy, Determination of the optical band gap for amorphous and nanocrystalline copper oxide thin films prepared by SILAR technique. *J. Phys. D Appl. Phys.* 42, 015413 (2009).
36. N.A. Raship, M.Z. Sahdan, F. Adriyanto, M.F. Nurfazliana, and A.S. Bakri, Effect of annealing temperature on the properties of copper oxide films prepared by dip coating technique. *AIP Conf. Proc.* 1788, 030121 (2017).
37. A.T. Fiory, *Encyclopedia of materials: science and technology*. ed. K. Buschow, R. Cahn, M. Flemings, B. Ilshner, E. Kramer, S. Mahajan, and P. Veyssiere (Oxford: Elsevier, 2001), p. 8009.
38. G. Martínez-Saucedo, R. Castanedo-Pérez, G. Torres-Delgado, J. Márquez-Marín, and O. Zelaya-Ángel, Cuprous oxide/cadmium stannate heterojunction diodes obtained by dip-coating method. *J. Alloys Compd.* 774, 153 (2019).
39. R. Bunea, A.K. Saikumar, and K. Sundaram, A comparison of optical properties of CuO and Cu₂O thin films for solar cell applications. *Mater. Sci. Appl.* 12, 315 (2021).
40. M.R. Dustgeer, S.T. Asma, A. Jilani, K. Raza, S.Z. Hussain, M.B. Shakoor, J. Iqbal, M.S. Abdel-wahab, and R. Darwesh, Synthesis and characterization of a novel single-phase sputtered Cu₂O thin films: structural, antibacterial activity and photocatalytic degradation of methylene blue. *Inorg. Chem. Commun.* 128, 108606 (2021).
41. P.B. Ahirrao, B.R. Sankapal, and R.S. Patil, Nanocrystalline p-type-cuprous oxide thin films by room temperature chemical bath deposition method. *J. Alloys Compd.* 509, 5551 (2011).
42. D. Ozaslan, O. Erken, M. Gunes, and C. Gumus, The effect of annealing temperature on the physical properties of Cu₂O thin film deposited by SILAR method. *Phys. B Condens. Matter.* 580, 411922 (2020).
43. G. Martínez-Saucedo, R. Castanedo-Pérez, G. Torres-Delgado, A. Mendoza-Galván, and O.Z. Ángel, Cuprous oxide thin films obtained by dip-coating method using rapid thermal annealing treatments. *Mater. Sci. Semicond. Process.* 68, 133 (2017).
44. S. Ishizuka, T. Maruyama, and K. Akimoto, Thin-film deposition of Cu₂O by reactive radio-frequency magnetron sputtering. *Jpn. J. Appl. Phys.* 39, L786 (2000).
45. D. Tahir, and S. Tougaard, Electronic and optical properties of Cu, CuO and Cu₂O studied by electron spectroscopy. *J. Phys. Condens. Matter* 24, 175002 (2012).
46. S. Budi, M. Takahashi, M.G. Sutrisno, W.A. Adi, Z. Fairuza, B. Kurniawan, S. Maenosono, and A.A. Umar, Phases evolution and photocatalytic activity of Cu₂O films electrodeposited from a non-pH-adjusted solution. *R. Soc. Open Sci.* 10, 230247 (2023).
47. J. Han, J. Chang, R. Wei, X. Ning, J. Li, Z. Li, H. Guo, and Y. Yang, Mechanistic investigation on tuning the conductivity type of cuprous oxide (Cu₂O) thin films via deposition potential. *Int. J. Hydrog. Energy* 43, 13764 (2018).
48. M. Kahk and J. Lischner, Core electron binding energies of adsorbates on Cu(111) from first-principles calculations. *Phys. Chem. Chem. Phys.* 20, 30403 (2018).
49. A. Barnasas, N. Kanistras, A. Ntagkas, D.I. Anyfantis, A. Stamatelatos, V. Kapaklis, N. Bouropoulos, E. Mystiridou, P. Pouloupoulos, C.S. Garoufalis, and S. Baskoutas, Quantum confinement effects of thin ZnO films by experiment and theory. *Phys. E* 120, 114072 (2020).
50. J.A. Switzer, C.J. Hung, E.W. Bohannon, M.G. Shumsky, T.D. Golden, and D.C. Van Aken, Electrodeposition of quantum-confined metal/semiconductor nano-composites. *Adv. Mater.* 9, 334 (1997).
51. Y. Chang, J.J. Teo, and H.C. Zeng, Formation of colloidal CuO nanocrystallites and their spherical aggregation and reductive transformation to hollow Cu₂O nanospheres. *Langmuir* 21, 1074 (2005).
52. K. Borgohain, N. Murase, and S. Mahamuni, Synthesis and properties of Cu₂O quantum particles. *J. Appl. Phys.* 92, 1292 (2002).
53. R. Len, H. Chen, T. Cui, Z. Zhang, Q. Zhou, L. Nan, W.C.M. Cheong, L. Schröck, V. Ramm, Q. Ding, X. Liang, S. Saris, F. Wendisch, S. Maier, R. Fischer, Y. Zhu, D. Wang, and E. Cortés, *ACS Catal.* 13, 11352 (2023).
54. P.L. Khoo, Y. Kikkawa, K. Satou, T. Shinagawa, and M. Izaki, Improvements in external quantum efficiency of electrochemically constructed n-ZnO/p-Cu₂O photovoltaic devices by rapid thermal annealing. *Thin Solid Films* 653, 158 (2017).
55. P.W. Kuo, J.H. Hsieh, W.T. Wu, and C.H. Wu, Optoelectronic properties of sputter-deposited Cu₂O-Ag-Cu₂O treated with rapid thermal annealing. *Vacuum* 84, 633 (2009).
56. K. Bergum, H.N. Riise, S. Gorantla, P.F. Lindberg, I. Jensen, A.E. Gunaes, A. Galeckas, S. Diplas, B.G. Svensson, and E. Monakhov, Improving carrier transport in Cu₂O thin films by rapid thermal annealing. *J. Phys. Condens. Matter* 30, 075702 (2018).

Publisher's Note Springer Nature remains neutral with regard to jurisdictional claims in published maps and institutional affiliations.